On the efficient computation of smoothness indicators for a class of WENO reconstructions

**Antonio Baeza · Raimund Bürger ·
Pep Mulet · David Zorío**

Abstract Common smoothness indicators used in Weighted Essentially Non-Oscillatory (WENO) reconstructions [Jiang, G.S., Shu, C.W.: Efficient implementation of Weighted ENO schemes, J. Comput. Phys. **126**, 202–228 (1996)] have quadratic cost with respect to the order. A set of novel smoothness indicators with linear cost of computation with respect to the order is presented. These smoothness indicators can be used in the context of schemes of the type introduced by Yamaleev and Carpenter [Yamaleev, N.K., Carpenter, M.H.: A systematic methodology to for constructing high-order energy stable WENO schemes. J. Comput. Phys. **228**(11), 4248–4272 (2009)]. The accuracy properties of the resulting nonlinear weights are the same as those arising from using the traditional Jiang-Shu smoothness indicators in Yamaleev-Carpenter-type reconstructions. The increase of the efficiency and ease of implementation are shown.

Keywords finite-difference schemes, WENO reconstructions, smoothness indicators

A. Baeza · P. Mulet
Departament de Matemàtiques
Universitat de València
E-46100 Burjassot, Spain
E-mail: antonio.baeza@uv.es, mulet@uv.es

R. Bürger
CI^{2}MA & Departamento de Ingeniería Matemática
Universidad de Concepción
Casilla 160-C, Concepción, Chile
E-mail: rburger@ing-mat.udec.cl

D. Zorío (**Corresponding author**)
CI^{2}MA, Universidad de Concepción
Casilla 160-C, Concepción, Chile
E-mail: dzorio@ci2ma.udec.cl

1 Introduction

1.1 Scope

Weighted Essentially Non-Oscillatory (WENO) schemes are a very useful and powerful tool to reconstruct functions from discrete data. They avoid an oscillatory behaviour in presence of a discontinuity and attain the optimal interpolation order whenever possible when the data is smooth. The most common contexts in which these schemes are used are finite-difference or finite-volume schemes discretizing hyperbolic conservation laws, whose solutions are typically non-smooth (weak solutions) and usually present strong shocks. WENO reconstructions are building blocks of numerical schemes that properly handle discontinuous solutions, and represent a popular way to construct high-order methods. However, it is well known that despite the recognized efficiency of these schemes, the most expensive part of the algorithm is the computation of local smoothness indicators, whose computational cost is quadratic with respect to the order of the scheme.

It is the purpose of this work to advance a novel design of smoothness indicators so that they are cheaper to compute (namely, at linear cost in terms of the order of accuracy) than the Jiang-Shu smoothness indicators [4] in the context of Yamaleev-Carpenter reconstructions [13], while both properties of optimal accuracy in case of smoothness and robust capture of discontinuities are ensured. To do so, we first advance theoretical considerations that are needed for their foundation, and that allow us to ultimately define the new smoothness indicators along with the associated weight design. The resulting WENO schemes are addressed as "Fast WENO" (FWENO) schemes.

1.2 Related work

The classical WENO schemes were proposed by Jiang and Shu [4,10] as an improvement of the original proposal of Liu et al. [6]. The idea is to build a weighted combination of interpolators, with the weights depending on smoothness indicators that tune the weight according to the data. The smoothness indicators defined by Jiang and Shu are designed in a way such that they take small values if the data used to construct the indicator is smooth and large values otherwise, with the additional property that the values of indicators constructed with smooth data are close to each other. This property is important as the order of accuracy of the final reconstruction is strongly dependent on it.

Several years later, Yamaleev and Carpenter [12] proposed a new third-order WENO scheme, which was later on extended to arbitrary order in [13] (henceforth, YC-WENO scheme). In this case, the non-linear weights are based instead on a ratio between a high-order undivided difference, which is very small when the data is smooth and large if a discontinuity crosses the data stencil, and the original Jiang-Shu smoothness indicators. In this latter case the accuracy of the scheme is based on the asymptotic convergence of the undivided difference and the smoothness indicators, rather than the closeness between the latter ones. This allows one to simplify the smoothness indicators, which is presented in this paper.

1.3 Outline of this paper

The remainder of the paper is organized as follows. In Section 2, we provide the theoretical background for the novel smoothness indicators. Section 3 is devoted to the definition of the smoothness indicators, the construction of the corresponding numerical scheme and the analysis of its accuracy. Section 4 contains several numerical experiments in which the new algorithm is compared against the previous ones in terms of accuracy and efficiency. Finally, in Section 5 some conclusions are drawn.

2 Preliminaries

2.1 Asymptotic properties of functions

We recall that for $\alpha \in \mathbb{Z}$,

$$f(h) = \mathcal{O}(h^\alpha) \Leftrightarrow \limsup_{h \to 0} \left| \frac{f(h)}{h^\alpha} \right| < \infty,$$

and define the more restrictive property

$$f(h) = \bar{\mathcal{O}}(h^\alpha) :\Leftrightarrow \limsup_{h \to 0} \left| \frac{f(h)}{h^\alpha} \right| < \infty \wedge \liminf_{h \to 0} \left| \frac{f(h)}{h^\alpha} \right| > 0.$$

For positive functions f and g, the properties

$$\limsup_{h \to 0} f(h)g(h) \le \limsup_{h \to 0} f(h) \limsup_{h \to 0} g(h),$$

$$\liminf_{h \to 0} f(h)g(h) \ge \liminf_{h \to 0} f(h) \liminf_{h \to 0} g(h)$$

imply that for $\alpha, \beta \in \mathbb{Z}$, $\mathcal{O}(h^\alpha)\mathcal{O}(h^\beta) = \mathcal{O}(h^{\alpha+\beta})$ and $\bar{\mathcal{O}}(h^\alpha)\bar{\mathcal{O}}(h^\beta) = \bar{\mathcal{O}}(h^{\alpha+\beta})$. Here and in what follows it is always understood that expressions of the form $\mathcal{O}(h^\alpha)$, $\bar{\mathcal{O}}(h^\alpha)$ correspond to $h \to 0$. Similarly, taking into account that for $A_i \subseteq (0, \infty)$, $\sup_i \inf A_i = \inf_i \sup A_i^{-1}$ where we define $A_i^{-1} := \{1/x \colon x \in A_i\}$, it follows that for a positive function f,

$$\liminf_{h \to 0} f(h) = \limsup_{h \to 0} f(h)^{-1},$$

therefore, if f is positive, then $f(h) = \bar{\mathcal{O}}(h^\alpha)$ implies $f(h)^{-1} = \bar{\mathcal{O}}(h^{-\alpha})$.

2.2 Point values and cell averages of smooth functions

Finite-difference and finite-volume schemes for hyperbolic conservation laws are based on discretizations of the solution by means of point values and cell averages, respectively. The following lemmas state the same result for both cases so that we can analyze them in a unified way.

Lemma 1 *Assume that a function $\varphi \in \mathcal{C}^{n+2}$ satisfies $\varphi^{(k)}(0) = 0$ for $k = 1, \ldots, n$ and $\varphi^{(n+1)}(0) \ne 0$. Then $\varphi(h) = \bar{\mathcal{O}}(h^{n+1})$.*

Proof The $(n+1)$-th order Taylor expansion of φ yields

$$\varphi(h) = \frac{\varphi^{(n+1)}(0)}{(n+1)!}h^{n+1} + \mathcal{O}(h^{n+2}),$$

which implies that

$$\lim_{h \to 0} \frac{\varphi(h)}{h^{n+1}} = \frac{\varphi^{(n+1)}(0)}{(n+1)!} \neq 0,$$

which in turn means that $\varphi(h) = \bar{\mathcal{O}}(h^{n+1})$. ∎

Lemma 2 *Let $c, d, z \in \mathbb{R}$. Assume that*

$$\begin{cases} f^{(k)}(z) = 0 \text{ for } k = 1, \ldots, n, \ f^{(n+1)}(z) \neq 0, \text{ and } f \in \mathcal{C}^{n+2} & \text{if } c + d \neq 0, \\ f^{(2k-1)}(z) = 0 \text{ for } k = 1, \ldots, m, \ f^{(2m+1)}(z) \neq 0, \text{ and } f \in \mathcal{C}^{2m+2} & \text{if } c + d = 0. \end{cases}$$

Then

$$f(z + dh) - f(z + ch) = \bar{\mathcal{O}}(h^\nu), \tag{2.1}$$

$$\frac{1}{h}\left(\int_{z+(d-1/2)h}^{z+(d+1/2)h} f(x)\,\mathrm{d}x - \int_{z+(c-1/2)h}^{z+(c+1/2)h} f(x)\,\mathrm{d}x \right) = \bar{\mathcal{O}}(h^\nu), \tag{2.2}$$

where

$$\nu = \begin{cases} n + 1 & \text{if } c + d \neq 0, \\ 2m + 1 & \text{if } c + d = 0. \end{cases}$$

Proof Our purpose is to apply Lemma 1 to the difference

$$\varphi(h) = f(z + dh) - f(z + ch)$$

to obtain (2.1) and alternatively, to the expression

$$\varphi(h) = \frac{1}{h}\left(\int_{z+(d-1/2)h}^{z+(d+1/2)h} f(x)\,\mathrm{d}x - \int_{z+(c-1/2)h}^{z+(c+1/2)h} f(x)\,\mathrm{d}x \right) \tag{2.3}$$

to obtain (2.2). For (2.1), it follows directly that

$$\varphi^{(k)}(0) = \mu(k, c, d) f^{(k)}(z), \quad \text{where } \mu(k, c, d) = d^k - c^k.$$

Since $c \neq d$ there clearly holds that $\mu(k, c, d) = 0$ if and only if k is even and $c + d = 0$.

For (2.2), we obtain from (2.3) multiplied by h

$$\big(h\varphi(h)\big)'(h) = -\left(d - \frac{1}{2}\right)f\left(z + \left(d - \frac{1}{2}\right)h\right) + \left(d + \frac{1}{2}\right)f\left(z + \left(d + \frac{1}{2}\right)h\right)$$
$$+ \left(c - \frac{1}{2}\right)f\left(z + \left(c - \frac{1}{2}\right)h\right) - \left(c + \frac{1}{2}\right)f\left(z + \left(c + \frac{1}{2}\right)h\right)$$

and for $k \geq 1$,

$$\big(h\varphi(h)\big)^{(k+1)}(0)$$

$$= \left(-\left(d - \frac{1}{2}\right)^{k+1} + \left(d + \frac{1}{2}\right)^{k+1} + \left(c - \frac{1}{2}\right)^{k+1} - \left(c + \frac{1}{2}\right)^{k+1} \right) f^{(k)}(z).$$

On the other hand, the Leibniz formula for higher derivatives yields

$$\left(h\varphi(h) \right)^{(k+1)}(0) = (k+1)\varphi^{(k)}(0).$$

Therefore, for $k \geq 1$ we get $\varphi^{(k)}(0) = \mu(k, c, d) f^{(k)}(z)$, where

$$\mu(k, c, d) = \frac{1}{k+1} \left(-\left(d - \frac{1}{2}\right)^{k+1} + \left(d + \frac{1}{2}\right)^{k+1} + \left(c - \frac{1}{2}\right)^{k+1} - \left(c + \frac{1}{2}\right)^{k+1} \right).$$

Since

$$\left(d + \frac{1}{2}\right)^{k+1} - \left(d - \frac{1}{2}\right)^{k+1} = \sum_{l=0}^{k+1} \binom{k+1}{l} d^{k+1-l} \left(\frac{1}{2^l} - \frac{(-1)^l}{2^l} \right)$$

$$= \sum_{s=0}^{\lfloor k/2 \rfloor} \binom{k+1}{2s+1} d^{k-2s} \frac{1}{2^{2s}},$$

we obtain

$$\mu(k, c, d) = \frac{1}{k+1} \sum_{s=0}^{\lfloor k/2 \rfloor} \binom{k+1}{2s+1} \frac{1}{2^{2s}} (d^{k-2s} - c^{k-2s}). \qquad (2.4)$$

Now, if $c = -d$, then $\mu(k, c, d) = 0$ if k is even and

$$\mu(k, -d, d) = \frac{1}{k+1} \sum_{s=0}^{\lfloor k/2 \rfloor} \binom{k+1}{2s+1} \frac{1}{2^{2s-1}} d^{k-2s} \neq 0$$

if k is odd, since the sign of all summands is the sign of d. On the other hand, if $c + d \neq 0$, since $c \neq d$, then $|c| \neq |d|$, so all summands in (2.4) have the same sign, which yields $\mu(k, c, d) \neq 0$ for any $k \geq 1$. Therefore $\mu(k, c, d) = 0$ if and only if k is odd and $c + d = 0$. In both cases it follows from the definition of n and m in the assumptions that

$$\begin{cases} \varphi^{(k)}(0) = 0 \text{ for } k = 1, \ldots, n, \ \varphi^{(n+1)}(0) \neq 0, \text{ and } \varphi \in \mathcal{C}^{n+2} & \text{if } c + d \neq 0, \\ \varphi^{(k)}(0) = 0 \text{ for } k = 1, \ldots, 2m, \ \varphi^{(2m+1)}(0) \neq 0, \text{ and } \varphi \in \mathcal{C}^{2m+2} & \text{if } c + d = 0, \end{cases}$$

so Lemma 1 yields the final result. ∎

3 Modified smoothness indicators and new weight design

In this section the modified WENO schemes with the new smoothness indicators are considered for YC-WENO-type schemes [13]. Schemes of order $2r-1$ are based on a stencil

$$S = \{f_{-r+1}, \ldots, f_{r-1}\}, \qquad (3.1)$$

where f_i results either from a point-value or a cell-average discretization of a function f:

$$f_i = \mathcal{L}[f](x_i) := \begin{cases} f(x_i) & \text{for point values,} \\ \dfrac{1}{h} \displaystyle\int_{x_i - h/2}^{x_i + h/2} f(\xi)\,\mathrm{d}\xi & \text{for cell averages} \end{cases}$$

for constant $h := x_{i+1} - x_i$, where we wish to reconstruct f at $x_{1/2}$. In the following sections we introduce the "Fast WENO" (FWENO) schemes.

3.1 Fast WENO (FWENO) schemes of order $2r - 1$, $r \geq 2$

The traditional Jiang-Shu smoothness indicators [4] are defined by

$$I_{r,i}^{\mathrm{JS}} := \sum_{k=1}^{r-1} \int_{x_{-1/2}}^{x_{1/2}} h^{2k-1} \big(p_{r,i}^{(k)}(x) \big)^2 \mathrm{d}x, \quad 0 \leq i \leq r - 1, \tag{3.2}$$

where $p_{r,i}$ are the corresponding interpolating polynomials associated to the sub-stencils $S_{r,i} = \{f_{-r+1+i}, \ldots, f_i\}$, $0 \leq i \leq r - 1$. These smoothness indicators have been typically used in the literature involving WENO schemes, although their evaluation is computationally expensive (quadratic with respect to the order, as becomes evident from the identity deduced from [1, Proposition 5] (see subsection 3.3 for a more efficient computation, but still quadratic in r):

$$I_{r,i}^{\mathrm{JS}} = \sum_{j=0}^{r-1} \sum_{k=0}^{j} e_{j,k} f_{-r+1+i+j} f_{-r+1+i+k}.$$

We propose new smoothness indicators for both (point-value and cell-average) reconstructions that have *linear* cost with respect to the order (namely, they involve $r - 2$ additions and $r - 1$ multiplications), and that are defined by

$$I_{r,i} := \sum_{j=1}^{r-1} (f_{-r+i+j+1} - f_{-r+i+j})^2, \quad 0 \leq i \leq r - 1. \tag{3.3}$$

A detailed analysis on the computational cost of the smoothness indicators in both cases is included in Section 3.3. The remaining parts of the algorithm are the same as those defined in [13] for the YC-WENO schemes. For the sake of exposition, we briefly describe it:

Input: $S = \{f_{-r+1}, \ldots, f_{r-1}\}$, with $f_i = \mathcal{L}[f](x_i)$, and $\varepsilon > 0$.

1. Compute interpolating polynomials

$$p_{r,i}(x) = \mathcal{I}_m(x_{-r+1+i}, \ldots, x_i; f_{-r+1+i}, \ldots, f_i; x), \quad 0 \leq i \leq r - 1,$$

   where $\mathcal{I}_m$ computes approximate point values from either point values or cell averages, according to the discretization.
2. Compute the new smoothness indicators (3.3).

3. Obtain the corresponding squared undivided differences of order $2r - 2$:

$$d_r = \left(\sum_{j=-r+1}^{r-1} (-1)^{j+r-1} \binom{2r-2}{j+r-1} f_j \right)^2. \tag{3.4}$$

4. Compute the terms

$$\alpha_{r,i} = c_{r,i} \left(1 + \frac{d_r^{s_1}}{I_{r,i}^{s_1} + \varepsilon} \right)^{s_2}, \quad 0 \le i \le r - 1, \tag{3.5}$$

where $c_{r,i}$ are the ideal linear weights, for some s_1, s_2 chosen by the user such that $s_1 \ge 1$ and $s_2 \ge \frac{r}{2s_1}$.

5. Generate the WENO weights:

$$\omega_{r,i} = \frac{\alpha_{r,i}}{\alpha_{r,0} + \cdots + \alpha_{r,r-1}}, \quad i = 0, \ldots, r - 1. \tag{3.6}$$

6. Obtain the reconstruction at $x_{1/2}$:

$$q_r(x_{1/2}) = \sum_{i=0}^{r-1} \omega_{r,i} p_{r,i}(x_{1/2}). \tag{3.7}$$

Output: $q_r(x_{1/2})$.

Remark 1 As stated above, the difference between our proposed WENO method and YC-WENO is the usage of the new smoothness indicators $I_{r,i}$ as defined in (3.3) in the former case and the usage of the classical smoothness indicators $I_{r,i}^{\mathrm{JS}}$ as defined in (3.2) in the latter case. In turn, the difference between JS-WENO and YC-WENO schemes is that in the former case the coefficients $\alpha_{r,i}$ are defined by

$$\alpha_{r,i} = \frac{c_{r,i}}{(I_{r,i}^{\mathrm{JS}} + \varepsilon)^s}, \quad s \ge r/2, \tag{3.8}$$

instead of (3.5).

3.2 Accuracy properties of FWENO schemes

We next analyze the accuracy properties of the novel smoothness indicators.

Lemma 3 *Let $r \ge 3$, and a grid be defined by $x_i = z + (c+i)h$ for $-r+1 \le i \le r-1$. Assume that S given by (3.1) is a stencil such that $f_i = \mathcal{L}[f](x_i)$, with $f^{(k)}(z) = 0$ for $1 \le k \le n$ and $f^{(n+1)}(z) \ne 0$, $f \in \mathcal{C}^{n+1}$, $n \in \mathbb{N} \cup \{0\}$, and assume that there exists $m \in \mathbb{N} \cup \{0\}$ such that $f^{(2m+1)}(z) \ne 0$. Furthermore, assume that the quantities $I_{r,i}$ are given by (3.3). Then $I_{r,i} = \bar{\mathcal{O}}(h^{2n+2})$.*

On the other hand, if $r \ge 2$ and f has a unique discontinuity located in (x_{-r+1}, x_{r-1}), then there exist indices i_0, i_1 with $-r+1 \le i_0, i_1 \le r-1$ such that $I_{r,i_0} = \bar{\mathcal{O}}(1)$ and $I_{r,i_1} = \mathcal{O}(h^2)$.

Proof If $c \notin \{1/2 + j \mid -r + 1 \leq j \leq r - 2\}$, then by Lemma 2 there holds

$$f_{j+1} - f_j = \bar{\mathcal{O}}(h^{n+1}) \Leftrightarrow (f_{j+1} - f_j)^2 = \bar{\mathcal{O}}(h^{2n+2}) \quad \text{for all } j = -r + 1, \ldots, r - 2.$$

Therefore, in particular, one has

$$I_{r,i} = \sum_{j=1}^{r-1} \bar{\mathcal{O}}(h^{2n+2}) = \bar{\mathcal{O}}(h^{2n+2}) \quad \text{for all } i = -r + 1, \ldots, r - 1.$$

Let us now assume that $c = 1/2 + j_0$ for some j_0, $-r + 1 \leq j_0 \leq r - 2$. Then, again by Lemma 2:

$$f_{j_0+1} - f_{j_0} = \bar{\mathcal{O}}(h^{2m+1});$$
$$f_{j+1} - f_j = \bar{\mathcal{O}}(h^{n+1}) \quad \text{for all } j = -r + 1, \ldots, r - 2, \ j \neq j_0.$$

Thus, we have the following: If $j_0 \notin \{-r + i + 1, \ldots, i - 1\}$, then

$$I_{r,i} = \sum_{j=1}^{r-1} \bar{\mathcal{O}}(h^{2n+2}) = \bar{\mathcal{O}}(h^{2n+2})$$

Otherwise, that is if $j_0 \in \{-r + i + 1, \ldots, i - 1\}$, we get

$$I_{r,i} = (f_{j_0+1} - f_{j_0})^2 + \sum_{j=1, j \neq j_0 + r - i}^{r-1} (f_{-r+i+j+1} - f_{-r+i+j})^2$$
$$= \bar{\mathcal{O}}(h^{4m+2}) + \sum_{j=1, j \neq j_0 + r - i}^{r-1} \bar{\mathcal{O}}(h^{2n+2}) = \bar{\mathcal{O}}(h^{4m+2}) + \bar{\mathcal{O}}(h^{2n+2}) = \bar{\mathcal{O}}(h^{2n+2}),$$

since clearly by definition $2m + 1 \geq n + 1$.

Finally, if f has a unique discontinuity at (x_{-r+1}, x_{r-1}), then there exists $j_1 \in \{-r + 1, \ldots, r - 2\}$ such that $f_{j_1+1} - f_{j_1} = \bar{\mathcal{O}}(1)$, whereas $f_{j+1} - f_j = \mathcal{O}(h)$ for $j_1 \neq j \in \{-r + 1, \ldots, r - 2\}$. Hence, if we select for instance $i_0 = 0$ and $i_1 = r - 1$ if $j_1 \geq 0$, or $i_0 = r - 1$ and $i_1 = 0$ if $j_1 < 0$, then clearly $I_{r,i_0} = \bar{\mathcal{O}}(1)$ and $I_{r,i_1} = \mathcal{O}(h^2)$. ■

Remark 2 The case $r = 2$ for the FWENO method is the same as in the original YC-WENO method, since in this case the proposed smoothness indicators are the same. In this case, the statement of Lemma 3 does not hold in general, since one can have $I_{2,i} = \mathcal{O}(h^{4m+2})$ if $c = 1/2 + i - 1$.

Theorem 1 *Under the same conditions and notation as in Lemma 3, with $r \geq 3$ and dropping the role of ε, there holds*

$$q_r(x_{1/2}) = \begin{cases} f(x_{1/2}) + \mathcal{O}(h^{2r-1}) & \text{if } n < 2r - 3, \\ f(x_{1/2}) + \mathcal{O}(h^{n+1}) & \text{if } n \geq 2r - 3, \\ f(x_{1/2}) + \mathcal{O}(h^r) & \text{if a discontinuity crosses the data.} \end{cases}$$

Proof We first assume smoothness with a critical point of order n. Then, by Lemma 3, the new smoothness indicators satisfy $I_{r,i} = \bar{\mathcal{O}}(h^{2n+2})$. We consider in first place the case $n < 2r - 3$. Then there holds for $\alpha_{r,i}$:

$$\alpha_{r,i} = c_{r,i}\left(1 + \frac{d_r^{s_1}}{I_{r,i}^{s_1}}\right)^{s_2} = c_{r,i}\left(1 + \frac{\mathcal{O}(h^{(4r-4)s_1})}{\bar{\mathcal{O}}(h^{(2n+2)s_1})}\right)^{s_2}$$

$$= c_{r,i}\left(1 + \mathcal{O}(h^{2(2r-3-n)s_1})\right)^{s_2} = c_{r,i} + \mathcal{O}(h^{2(2r-3-n)s_1}).$$

Hence, the non-linear weights satisfy

$$\omega_{r,i} = \frac{\alpha_{r,i}}{\sum_{j=0}^{r-1}\alpha_{r,j}} = \frac{c_{r,i} + \mathcal{O}(h^{2(2r-3-n)s_1})}{\sum_{j=0}^{r-1}\left(c_{r,i} + \mathcal{O}(h^{2(2r-3-n)s_1})\right)} = \frac{c_{r,i} + \mathcal{O}(h^{2(2r-3-n)s_1})}{\sum_{j=0}^{r-1}c_{r,i} + \mathcal{O}(h^{2(2r-3-n)s_1})}$$

$$= \frac{c_{r,i} + \mathcal{O}(h^{2(2r-3-n)s_1})}{1 + \mathcal{O}(h^{2(2r-3-n)s_1})} = c_{r,i} + \mathcal{O}(h^{2(2r-3-n)s_1}).$$

On the other hand, $p_{r,i}(x_{1/2}) = f(x_{1/2}) + \mathcal{O}(h^M)$ with $M := \max\{r, n+1\}$. Therefore, denoting by

$$p_r(x_{1/2}) := \sum_{i=0}^{r-1} c_{r,i} p_{r,i}(x_{1/2})$$

the value at $x_{1/2}$ of the optimal $(2r-1)$-th order polynomial, we have

$$q_r(x_{1/2}) - f(x_{1/2}) = q_r(x_{1/2}) - p_r(x_{1/2}) + p_r(x_{1/2}) - f(x_{1/2})$$

$$= \sum_{i=0}^{r-1}\omega_{r,i}p_{r,i}(x_{1/2}) - \sum_{i=0}^{r-1}c_{r,i}p_{r,i}(x_{1/2}) + \left(p_r(x_{1/2}) - f(x_{1/2})\right)$$

$$= \sum_{i=0}^{r-1}(\omega_{r,i} - c_{r,i})p_{r,i}(x_{1/2}) + \mathcal{O}(h^{2r-1})$$

$$= \sum_{i=0}^{r-1}(\omega_{r,i} - c_{r,i})\left(p_{r,i}(x_{1/2}) - f(x_{1/2})\right) + \mathcal{O}(h^{2r-1})$$

$$= \sum_{i=0}^{r-1}\mathcal{O}(h^{2(2r-3-n)s_1})\mathcal{O}(h^M) + \mathcal{O}(h^{2r-1})$$

$$= \mathcal{O}(h^{2(2r-3-n)s_1+M}) + \mathcal{O}(h^{2r-1}).$$

Taking into account that $s_1 \geq 1$, we have

$$q_r(x_{1/2}) - f(x_{1/2}) = \mathcal{O}(h^{2(2r-3-n)+M}) + \mathcal{O}(h^{2r-1}).$$

We next analyze the exponent of the left summand, splitting the discussion into two cases. On one hand, if $n \leq r - 1$, then $M = r$ and there holds

$$2(2r-3-n)+M = 2(2r-3-n)+r = 5r-6-2n \geq 5r-6-2(r-1) = 3r-4 \geq 2r-1,$$

where the last inequality holds since by assumption $r \geq 3$.

On the other hand, if $n \geq r - 1$, then $M = n + 1$ and then, since by assumption $n \leq 2r - 4$,

$$2(2r - 3 - n) + M = 2(2r - 3 - n) + (n + 1) = 4r - 5 - n \geq 4r - 5 - (2r - 4) = 2r - 1.$$

Thus, for the case $n < 2r - 3$ there holds $q_r(x_{1/2}) - f(x_{1/2}) = \mathcal{O}(h^{2r-1})$.

In second place, we assume now $n \geq 2r - 3$, then, using that $\sum_{i=0}^{r-1} \omega_{r,i} = 1$, there holds

$$q_r(x_{1/2}) = \sum_{i=0}^{r-1} \omega_{r,i} p_{r,i}(x_{1/2}) = \sum_{i=0}^{r-1} \omega_{r,i} \big(f(x_{1/2}) + \mathcal{O}(h^{n+1}) \big)$$

$$= \sum_{i=0}^{r-1} \omega_{r,i} f(x_{1/2}) + \mathcal{O}(h^{n+1}) = f(x_{1/2}) + \mathcal{O}(h^{n+1}).$$

Finally, if a discontinuity crosses the data, assume that J_0 is the set of indices associated to the substencils $S_{r,i}$, $i \in J_0$, in which the discontinuity is not crossed ($J_0 \neq \varnothing$ by the second part of Lemma 3), and J_1 the set of the remaining whose corresponding substencils $S_{r,i}$, $i \in J_1$, are crossed by the discontinuity. Then if $i \in J_0$,

$$\alpha_i = c_{r,i} \left(1 + \frac{d_r^{s_1}}{I_{r,i}^{s_1}} \right)^{s_2} = c_{r,i} \left(1 + \frac{\bar{\mathcal{O}}(1)}{\bar{\mathcal{O}}(h^{2s_1(n+1)})} \right)^{s_2} = \bar{\mathcal{O}}(h^{-2s_1 s_2(n+1)}),$$

and if $i \in J_1$,

$$\alpha_i = c_{r,i} \left(1 + \frac{d_r^{s_1}}{I_{r,i}^{s_1}} \right)^{s_2} = c_{r,i} \left(1 + \frac{\bar{\mathcal{O}}(1)}{\bar{\mathcal{O}}(1)} \right)^{s_2} = \bar{\mathcal{O}}(1).$$

Therefore, if $i \in J_0$,

$$\omega_i = \frac{\alpha_i}{\sum_{j=0}^{r-1} \alpha_j} = \frac{\alpha_i}{\sum_{j \in J_0} \alpha_j + \sum_{j \in J_1} \alpha_j}$$

$$= \frac{\bar{\mathcal{O}}(h^{-2s_1 s_2(n+1)})}{\sum_{j \in J_0} \bar{\mathcal{O}}(h^{-2s_1 s_2(n+1)}) + \sum_{j \in J_1} \bar{\mathcal{O}}(1)} = \frac{\bar{\mathcal{O}}(h^{-2s_1 s_2(n+1)})}{\bar{\mathcal{O}}(h^{-2s_1 s_2(n+1)})} = \mathcal{O}(1),$$

and if $i \in J_1$,

$$\omega_i = \frac{\alpha_i}{\sum_{j=0}^{r-1} \alpha_j} = \frac{\alpha_i}{\sum_{j \in J_0} \alpha_j + \sum_{j \in J_1} \alpha_j}$$

$$= \frac{\bar{\mathcal{O}}(1)}{\sum_{j \in J_0} \bar{\mathcal{O}}(h^{-2s_1 s_2(n+1)}) + \sum_{j \in J_1} \bar{\mathcal{O}}(1)} = \frac{\bar{\mathcal{O}}(1)}{\bar{\mathcal{O}}(h^{-2s_1 s_2(n+1)})} = \mathcal{O}(h^{2s_1 s_2(n+1)}).$$

Thus, we conclude that

$$q_r(x_{1/2}) - f(x_{1/2}) = \sum_{i=0}^{r-1} \omega_{r,i} p_{r,i}(x_{1/2}) - \sum_{i=0}^{r-1} \omega_{r,i} f(x_{1/2})$$

$$= \sum_{i=0}^{r-1} \omega_{r,i} \big(p_{r,i}(x_{1/2}) - f(x_{1/2}) \big)$$

$$\begin{aligned}
&= \sum_{i \in J_0} \omega_{r,i}\big(p_{r,i}(x_{1/2}) - f(x_{1/2})\big) + \sum_{i \in J_1} \omega_{r,i}\big(p_{r,i}(x_{1/2}) - f(x_{1/2})\big) \\
&= \sum_{i \in J_0} \mathcal{O}(1)\mathcal{O}(h^r) + \sum_{i \in J_1} \mathcal{O}(h^{2s_1 s_2 (n+1)})\mathcal{O}(1) \\
&= \mathcal{O}(h^r) + \mathcal{O}(h^{2s_1 s_2 (n+1)}).
\end{aligned}$$

Now using that $n \geq 0$ and $s_2 \geq \frac{r}{2s_1}$, we have

$$2s_1 s_2 (n+1) \geq 2s_1 \frac{r}{2s_1} = r.$$

Therefore $q_r(x_{1/2}) - f(x_{1/2}) = \mathcal{O}(h^r)$, which completes the proof. ∎

Remark 3 According to this result, the only case in which our method loses accuracy with respect to the reconstruction with ideal linear weights is when $n = 2r-3$, in which the accuracy order decays to $2r-2$, namely, one unit less than the optimal accuracy order, $2r-1$.

3.3 Efficiency properties of FWENO schemes

We conclude this section with a comparison involving the number of operations of an FWENO interpolator with respect to the traditional JS-WENO and YC-WENO interpolators. In order to do so, we invoke [1, Propositions 1 and 5] to conclude that the evaluation of the reconstruction polynomials at the reconstruction point and the classical Jiang-Shu smoothness indicators can be respectively written as

$$p_{r,i}(x_{1/2}) = \sum_{j=0}^{r-1} d_{i,j} f_{-r+1+i+j},$$

$$I_{r,i}^{\text{JS}} = \sum_{j=0}^{r-1} \sum_{k=0}^{j} e_{i,j,k} f_{-r+1+i+j} f_{-r+1+i+k}, \quad 0 \leq i \leq r-1,$$

where $d_{i,j}, e_{i,j,k} \in \mathbb{R}$ are constants with respect to the data from the stencil.

This expression can be further simplified by taking into account that $I_{r,i}^{\text{JS}}$ is a positive semi-definite quadratic form defined on $(f_{-r+1+i}, \ldots, f_i)$ with rank $r-1$, therefore it can be expressed in a more convenient and numerically stable manner as a sum of squares of linear combinations of $f_{-r+1+i}, \ldots, f_i$. Specifically, for each $i = 0, \ldots, r-1$, let A_i be the matrix associated to $I_{r,i}^{\text{JS}}$, i.e.

$$I_{r,i}^{\text{JS}} = (f_{-r+1+i}, \ldots, f_i) A_i \begin{pmatrix} f_{-r+1+i} \\ \vdots \\ f_i \end{pmatrix}.$$

The $r \times r$ matrix A_i is semi-positively-definite with rank $r-1$ and therefore admits a decomposition as $A_i = P_i^{\text{T}} L_i D_i L_i^{\text{T}} P_i$, where P_i is a permutation matrix associated to the permutation σ_i of $(1, \ldots, r)$, L_i is lower triangular with unit entries in the

diagonal and $D_i = \text{diag}(\beta_{i,1}, \ldots, \beta_{i,r-1}, 0)$, with $\beta_{i,j} > 0$, $j = 1, \ldots, r-1$. This yields the following simplified expression:

$$I_{r,i}^{\text{JS}} = (f_{-r+1+i}, \ldots, f_i) P_i^{\text{T}} L_i D_i L_i^{\text{T}} P_i \begin{pmatrix} f_{-r+1+i} \\ \vdots \\ f_i \end{pmatrix}$$

$$= \sum_{j=1}^{r-1} \beta_{i,j} \left(\sum_{k=0}^{j} \gamma_{i,j,k} f_{i-r+\sigma_i(1+k)} \right)^2, \quad \gamma_{i,j,k} = (L_i)_{j,k}, \gamma_{i,j,j} = 1.$$

The cost associated to each reconstruction of lower order is thus $r-1$ additions and r multiplications, while the cost associated to each classical smoothness indicators is $(r^2+r-4)/2$ additions and $(r^2+3r-4)/2$ multiplications. Hence, the cost associated to the computation of the whole set of r reconstructions of lower order is $(r-1)r$ additions and r^2 multiplications, whereas the cost associated to the computation of the whole set of r classical smoothness indicators is $r(r^2+r-4)/2$ additions and $r(r^2 + 3r - 4)/2$ multiplications.

Now let us analyze the cost associated with the FWENO smoothness indicators (3.3). In this case, we also can reduce the number of operations by taking into consideration that the novel smoothness indicators satisfy a simple recurrence relation, in a way that their computation can be simplified in the following algorithm, involving a linear cost both in terms of additions and in terms of multiplications:

1. Compute
$$\theta_j := (f_{-r+j+1} - f_{-r+j})^2, \quad 1 \le j \le 2r - 2.$$

   Operations: $2r - 2$ additions and $2r - 2$ multiplications.
2. Compute
$$I_0 = \sum_{j=1}^{r-1} \theta_j.$$

   Operations: $r - 2$ additions.
3. Compute
$$I_i = I_{i-1} - \theta_i + \theta_{i+r-1}, \quad 1 \le i \le r - 1.$$

   Operations: $2r - 2$ additions.

Therefore, the cost associated to the whole set of smoothness indicators involves $5r - 6$ additions and $2r - 2$ multiplications.

Now, YC-WENO and FWENO schemes also involve the computation of (3.4), which involves $2r - 2$ additions and $2r$ multiplications.

As for the terms $\alpha_{r,i}$, we have two cases: for JS-WENO schemes, the expression for them is (3.8), and therefore the number of operations for each one is one addition, $s - 1$ multiplications and one division; therefore, the total cost for all them is r additions, $(s - 1)r$ multiplications and r divisions. As for YC-WENO and FWENO schemes, the expression to be computed is (3.5), and the number of operations associated to each one of them is two additions, $2s_1 + s_2 - 2$ multiplications and one division, being thus the total cost $2r$ additions, $(2s_1 + s_2 - 2)r$ multiplications and r divisions.

The non-linear weights $\omega_{r,i}$ have the same expression (3.6) in all cases. The denominator is the same for all the weights, and therefore one can previously

Order $2r-1$	JS-WENO		
Operations	Additions	Multiplications	Divisions
$p_r(x_{\frac{1}{2}})$	$(r-1)r$	r^2	0
I_r	$(r^3+r^2-4r)/2$	$(r^3+3r^2-4r)/2$	0
α_r	r	$(s-1)r$	r
ω_r	$r-1$	r	1
$q_r(x_{1/2})$	$r-1$	r	0
SUM	$(r^3+3r^2-4)/2$	$(r^3+5r^2+(2s-2)r)/2$	$r+1$
TOTAL	$r^3+4r^2+(s-1)r-2$		

Table 1: Theoretical cost for JS-WENO interpolator.

Order $2r-1$	YC-WENO		
Operations	Additions	Multiplications	Divisions
$p_r(x_{\frac{1}{2}})$	$(r-1)r$	r^2	0
I_r	$(r^3+r^2-4r)/2$	$(r^3+3r^2-4r)/2$	0
d_r	$2r-2$	$2r$	0
α_r	$2r$	$(2s_1+s_2-2)r$	r
ω_r	$r-1$	r	1
$q_r(x_{1/2})$	$r-1$	r	0
SUM	$(r^3+3r^2+6r-8)/2$	$(r^3+5r^2+(4s_1+2s_2)r)/2$	$r+1$
TOTAL	$r^3+4r^2+(2s_1+s_2+3)r-4$		

Table 2: Theoretical cost for YC-WENO interpolator.

store the value of $\bar{\alpha}_i := 1/(\sum_{j=0}^{r-1} \alpha_{i,j})$ and then compute $\omega_{r,i} = \alpha_{r,i}\bar{\alpha}_i$, converting thus r divisions, much more expensive than multiplications, in to one division and r multiplications. Therefore, the total cost corresponds now to $r-1$ additions and one division associated with the computation of $\bar{\alpha}_i$ and r multiplications (one multiplication per weight). Finally, the reconstruction expression (3.7) is also common in the three schemes, and corresponds to $r-1$ additions and r multiplications.

The number of operations associated to each term and the grand total of operations for each method is summarized in Tables 1 to 3, where it can be drawn as a conclusion that the number of operations of JS-WENO and YC-WENO is cubic with respect to the order, whereas the number of operations associated to FWENO increases quadratically with respect to the order. Therefore, the complexity of the smoothness indicators is indeed a crucial factor in terms of the impact on the computational cost, and using simplified alternatives can indeed reduce significantly the overall computational cost of the WENO interpolator.

A graphical comparison between the cost associated to each scheme is also shown in Figure 1, with $s = r/2$, $s_1 = r/2$ and $s_2 = 1$.

4 Numerical experiments

We now present some numerical experiments for schemes based on finite differences, as introduced in [8,9], combined with high-order WENO reconstructions to discretize hyperbolic conservation laws. Results obtained by the new FWENO scheme are compared with those generated by the JS-WENO and YC-WENO schemes. The exponent s for JS-WENO method is chosen as $s = \lceil r/2 \rceil$, while the

Order $2r-1$	FWENO		
Operations	Additions	Multiplications	Divisions
$p_r(x_{\frac{1}{2}})$	$(r-1)r$	r^2	0
I_r	$5r-6$	$2r-2$	0
d_r	$2r-2$	$2r$	0
α_r	$2r$	$(2s_1+s_2-2)r$	r
ω_r	$r-1$	r	1
$q_r(x_{1/2})$	$r-1$	r	0
SUM	$r^2+10r-10$	$r^2+(2s_1+s_2+4)r-2$	$r+1$
TOTAL	$2r^2+(2s_1+s_2+14)r-12$		

Table 3: Theoretical cost for FWENO interpolator.
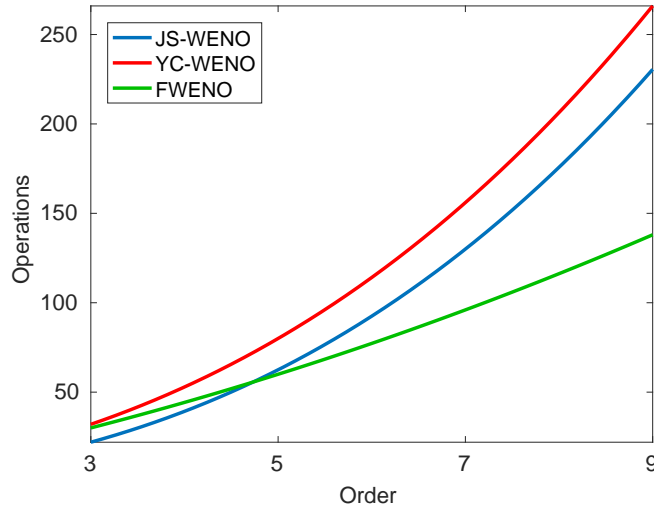
Fig. 1: Theoretical cost comparison between WENO interpolators.

exponents s_1 and s_2 for both YC-WENO and FWENO methods are chosen as $s_1 = \lceil r/2 \rceil$ and $s_2 = 1$. Finally, we set in all the numerical experiments $\varepsilon = 10^{-100}$, so that this parameter has the sole role of avoiding divisions by zero.

4.1 1D conservation law experiments

Example 1: Linear advection equation

We first apply the fifth-order accurate YC-WENO5 and FWENO schemes to the initial-boundary value problem for the linear advection equation

$$u_t + u_x = 0, \quad \Omega = (-1, 1), \quad u(-1, t) = u(1, t),$$
$$u_0(x) = 0.25 + 0.5\sin(\pi x),$$

which has the solution $u(x, t) = 0.25 + 0.5\sin(\pi(x-t))$. We run several simulations with final time $T = 1$ and grid spacings $h = 2/N$ and measure the resulting errors

	$\|\cdot\|_1$		$\|\cdot\|_\infty$		$\|\cdot\|_1$		$\|\cdot\|_\infty$	
	YC-WENO5				FWENO5			
N	Err.	$\mathcal{O}$	Err.	$\mathcal{O}$	Err.	$\mathcal{O}$	Err.	$\mathcal{O}$
10	1.02e-03	—	1.55e-03	—	1.01e-03	—	1.66e-03	—
20	3.27e-05	4.96	5.16e-05	4.91	3.27e-05	4.95	5.16e-05	5.01
40	1.01e-06	5.01	1.60e-06	5.01	1.01e-06	5.01	1.60e-06	5.01
80	3.15e-08	5.01	4.94e-08	5.01	3.15e-08	5.01	4.94e-08	5.01
160	9.79e-10	5.01	1.54e-09	5.01	9.79e-10	5.01	1.54e-09	5.01
320	3.05e-11	5.00	4.79e-11	5.00	3.05e-11	5.00	4.79e-11	5.00
640	9.52e-13	5.00	1.50e-12	5.00	9.53e-13	5.00	1.50e-12	5.00

Table 4: Example 1 (linear advection equation): fifth-order schemes with the new smoothness indicators.

	$\|\cdot\|_1$		$\|\cdot\|_\infty$		$\|\cdot\|_1$		$\|\cdot\|_\infty$	
	YC-WENO5				FWENO5			
N	Err.	$\mathcal{O}$	Err.	$\mathcal{O}$	Err.	$\mathcal{O}$	Err.	$\mathcal{O}$
40	2.44e-05	4.95	2.52e-04	4.70	2.73e-05	5.11	2.50e-04	4.69
80	7.89e-07	5.08	9.70e-06	5.05	7.89e-07	5.08	9.70e-06	5.05
160	2.32e-08	5.05	2.94e-07	5.03	2.32e-08	5.05	2.94e-07	5.03
320	7.01e-10	5.04	8.96e-09	5.03	7.01e-10	5.04	8.96e-09	5.03
640	2.14e-11	5.02	2.73e-10	5.02	2.14e-11	5.02	2.73e-10	5.02
1280	6.59e-13	5.02	8.41e-12	5.00	6.59e-13	5.02	8.41e-12	5.00

Table 5: Example 2 (Burgers equation): fifth-order schemes with the new smoothness indicators.

both in the L^1 and L^∞ norms. From the numerical results, which are shown in Table 4, one can conclude that both schemes converge numerically at approximate fifth-order rate, which is consistent with our theoretical analysis. In fact, the results for the YC-WENO and FWENO schemes are nearly identical.

Example 2: Burgers equation

We now solve numerically the following initial-boundary value problem for the inviscid Burgers equation:

$$u_t + (u^2/2)_x = 0, \quad \Omega = (-1, 1), \quad u(-1, t) = u(1, t),$$
$$u_0(x) = 0.25 + 0.5\sin(\pi x).$$

A first simulation is run until $T = 0.3$, in which the solution remains smooth. We compare both YC-WENO and FWENO schemes in the results shown in Table 5, where it can be observed that both methods attain again fifth order accuracy, producing an almost identical error.

The simulation is now run until $T = 12$. At $t = 1$, the wave breaks and a shock is generated. Therefore, we use the Donat-Marquina flux-splitting algorithm [3]. The results shown in Figure 2 correspond to the fifth-order schemes, with a resolution of $N = 80$ cells, and are compared with a reference solution computed with $N = 16000$ cells. The results obtained for all three methods are very similar, and therefore one can conclude that in this case using the new smoothness indicators does not appreciably affect the quality of the solution.
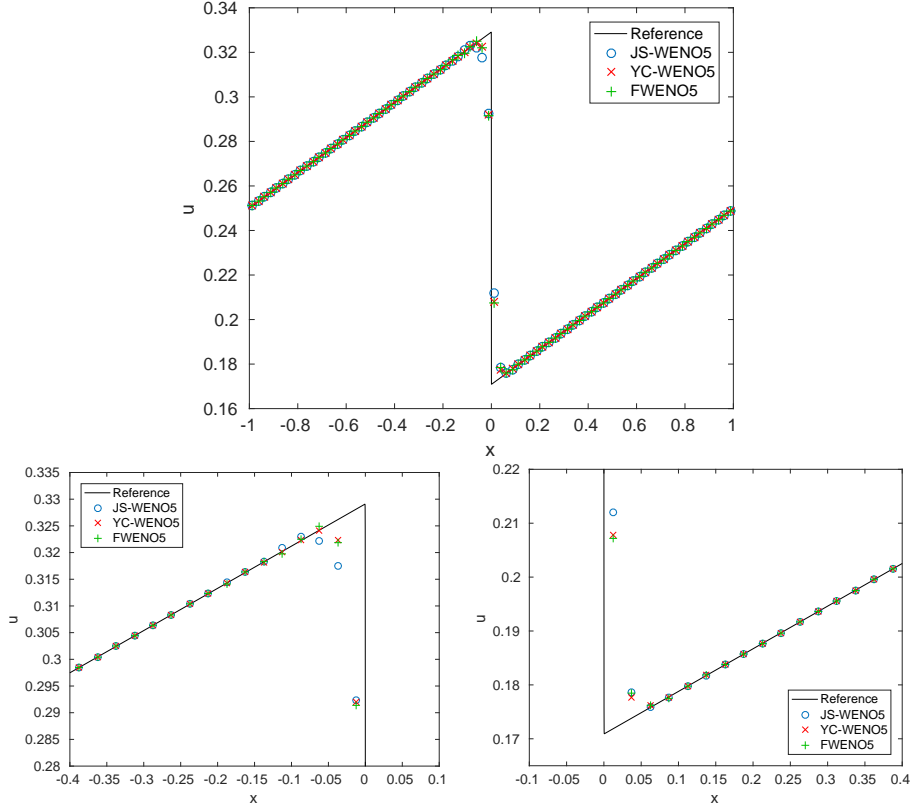
Fig. 2: Example 2 (inviscid Burgers equation): numerical solution for $N = 80$ (top) and enlarged views (bottom left and right) at $T = 12$ produced by fifth-order schemes with conventional (JS-WENO5 and YC-WENO5) and new (FWENO5) smoothness indicators. The reference solution with $N = 16000$ cells is also shown.

Example 3: Shu-Osher problem, 1D Euler equations of gas dynamics

The 1D Euler equations for gas dynamics are given by $\boldsymbol{u} = (\rho, \rho v, E)^{\mathrm{T}}$ and $\boldsymbol{f}(\boldsymbol{u}) = \boldsymbol{f}^1(\boldsymbol{u}) = (\rho v, p + \rho v^2, v(E + p))^{\mathrm{T}}$, where ρ is the density, v is the velocity and E is the specific energy of the system. The variable p stands for the pressure and is given by the equation of state

$$ p = (\gamma - 1)\left(E - \frac{1}{2}\rho v^2\right), $$

where γ is the adiabatic constant that will be taken as $\gamma = 1.4$. The spatial domain is $\Omega := (-5, 5)$, and the initial condition

$$ (\rho, v, p)(x, 0) = \begin{cases} \left(\dfrac{27}{7}, \dfrac{4\sqrt{35}}{9}, \dfrac{31}{3}\right) & \text{if } x \le -4, \\[2ex] \left(1 + \dfrac{1}{5}\sin(5x), 0, 1\right) & \text{if } x > -4, \end{cases} $$
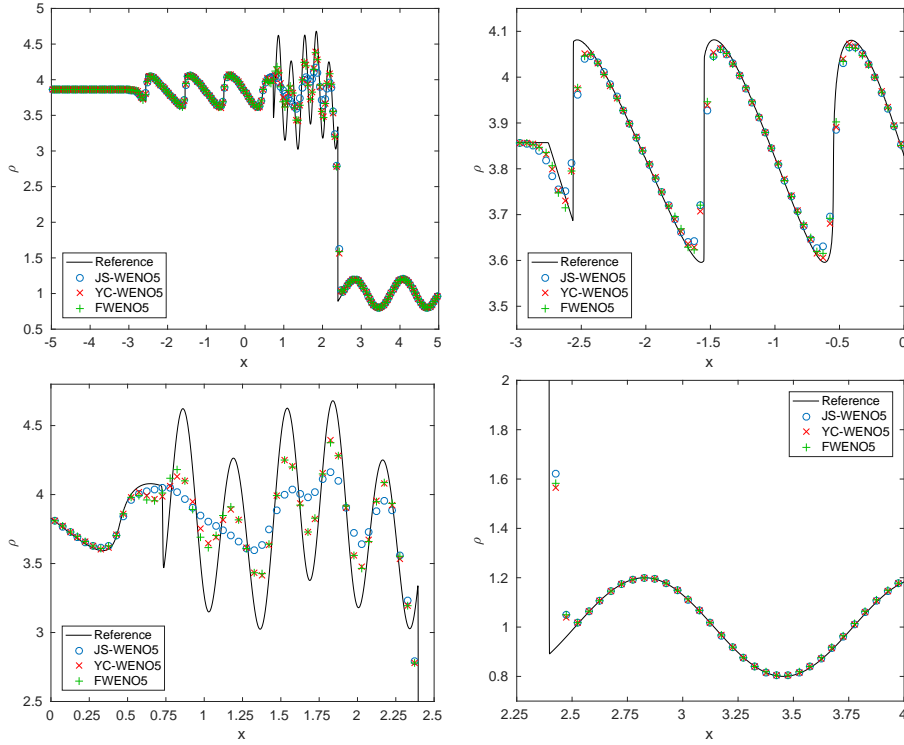
Fig. 3: Example 3 (Shu-Osher problem, 1D Euler equations of gas dynamics): numerical solution for $N = 200$ (top left) and enlarged views (top right, bottom left and bottom right) at $T = 1.8$ produced by fifth-order schemes with conventional (JS-WENO5 and YC-WENO5) and new (FWENO5) smoothness indicators. The reference solution with $N = 16000$ cells is also shown.

stipulates the interaction of a Mach 3 shock with a sine wave and is complemented with left inflow and right outflow boundary conditions. We run the simulation until $T = 1.8$ and compare the schemes against a reference solution computed with a resolution of $N = 16000$. Figures 3 and 4 display the results obtained by fifth-order schemes with resolutions of $N = 200$ and $N = 400$ cells, respectively. The results are similar for the YC-WENO and FWENO schemes and are slightly less sharply resolved for the JS-WENO scheme. In order to highlight the superior performance of the FWENO scheme, we also plot the numerical error against the CPU time for schemes of order $2r - 1$, with $3 \leq r \leq 5$, which is shown in Figures 5–7. These results clearly indicate that the scheme with the new smoothness indicators is more efficient (in terms of error reduction versus CPU time) than the schemes that employ the traditional Jiang-Shu smoothness indicators.
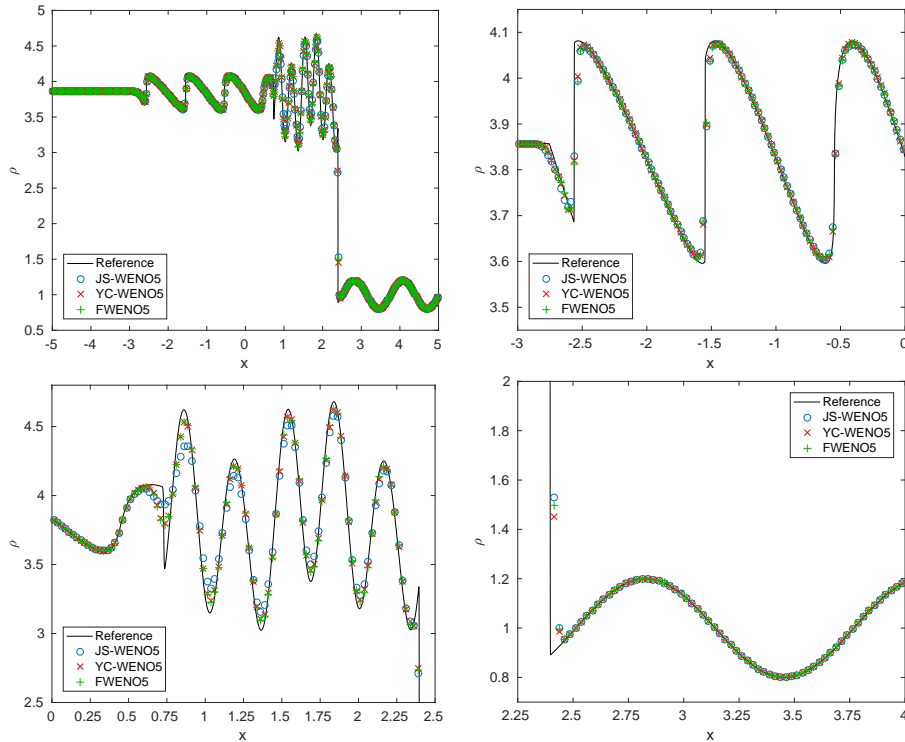
Fig. 4: Example 3 (Shu-Osher problem, 1D Euler equations of gas dynamics): numerical solution for $N = 400$ (top left) and enlarged views (top right, bottom left and bottom right) at $T = 1.8$ produced by fifth-order schemes with conventional (JS-WENO5 and YC-WENO5) and new (FWENO5) smoothness indicators. The reference solution with $N = 16000$ cells is also shown.

Example 4 (Sod shock tube problem, 1D Euler equations of gas dynamics)

We now apply WENO schemes to the 1D Euler equations of gas dynamics on $\Omega = (0, 1)$ with the initial condition

$$(\rho, v, p)(x, 0) = \begin{cases} (1, 0, 1) & \text{if } x \leq 0.5, \\ (0.125, 0, 0.1) & \text{if } x > 0.5 \end{cases}$$

and left and right Dirichlet boundary conditions corresponding to the shock tube problem proposed by Sod [11]. This problem has been tackled in many other papers afterwards, such as in [2]. The numerical result is produced by ninth-order schemes with a resolution of $N = 200$ cells compared against a reference solution which has been computed with a resolution of $N = 100000$ by the classical JS-WENO scheme. The simulation is run until $T = 0.1$ and the results are depicted in Figure 8. It turns our that the schemes produce very similar results. In fact, the most remarkable differences are favorable to our proposed FWENO scheme, since the behavior is slightly less oscillatory near the contact discontinuity and
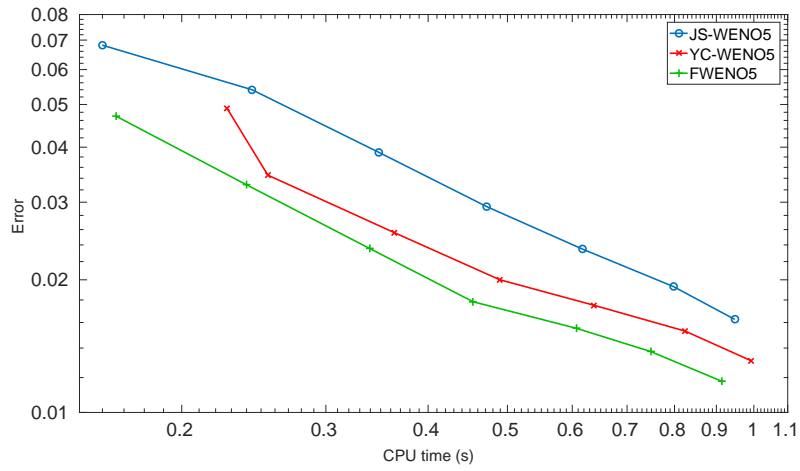
Fig. 5: Example 3 (Shu-Osher problem, 1D Euler equations of gas dynamics): efficiency plot for fifth-order schemes, corresponding to the numerical solution at $T = 1.8$.
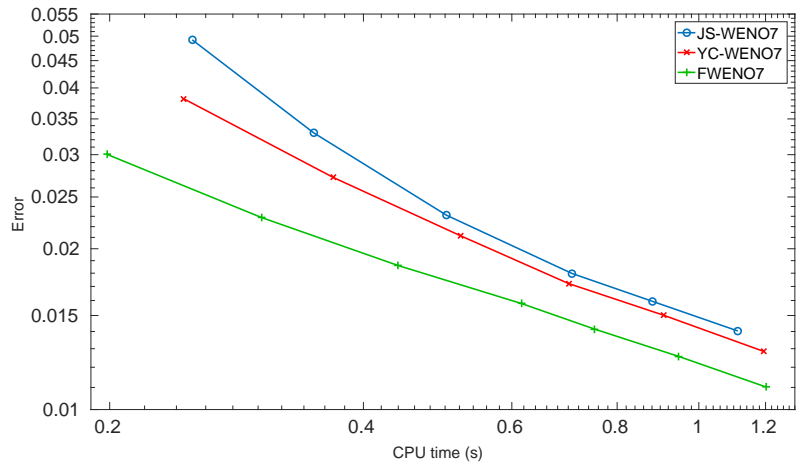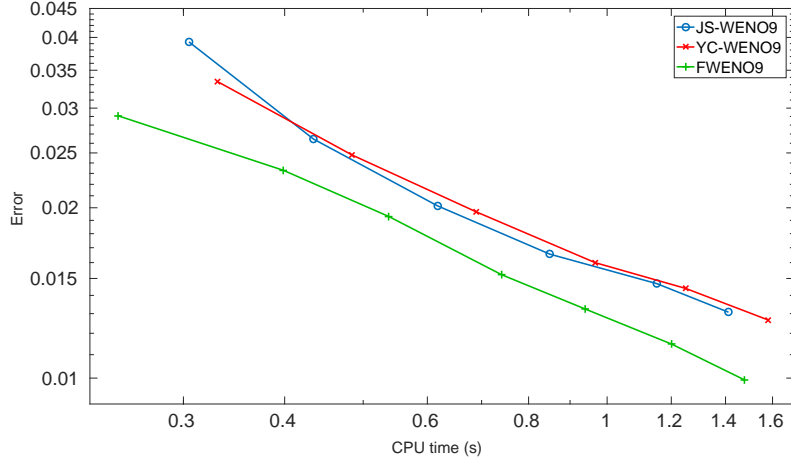

Fig. 6: Example 3: (Shu-Osher problem, 1D Euler equations of gas dynamics): efficiency plot for seventh-order schemes, corresponding to the numerical solution at $T = 1.8$.

the shock. Finally, an efficiency comparison is presented in Figure 9, where it can be concluded that our FWENO scheme turns out to be again more efficient than their classical JS-WENO and YC-WENO counterparts.

Fig. 7: Example 3: (Shu-Osher problem, 1D Euler equations of gas dynamics): efficiency plot for ninth-order schemes, corresponding to the numerical solution at $T = 1.8$.

4.2 2D conservation law experiments

Example 5 (double Mach reflection, 2D Euler equations of gas dynamics)

The two-dimensional Euler equations for inviscid gas dynamics are given by

$$\boldsymbol{u}_t + \boldsymbol{f}^1(\boldsymbol{u})_x + \boldsymbol{f}^2(\boldsymbol{u})_y = 0,$$

with

$$\boldsymbol{u} = \begin{pmatrix} \rho \\ \rho v^x \\ \rho v^y \\ E \end{pmatrix}, \quad \boldsymbol{f}^1(\boldsymbol{u}) = \begin{pmatrix} \rho v^x \\ p + \rho(v^x)^2 \\ \rho v^x v^y \\ v^x(E+p) \end{pmatrix}, \quad \boldsymbol{f}^2(\boldsymbol{u}) = \begin{pmatrix} \rho v^y \\ \rho v^x v^y \\ p + \rho(v^y)^2 \\ v^y(E+p) \end{pmatrix}.$$

Here ρ is the density, (v^x, v^y) is the velocity, E is the specific energy, and p is the pressure that is given by the equation of state

$$p = (\gamma - 1)\left(E - \frac{1}{2}\rho((v^x)^2 + (v^y)^2)\right),$$

where the adiabatic constant is again chosen as $\gamma = 1.4$. This experiment uses these equations to model a vertical right-going Mach 10 shock colliding with an equilateral triangle. By symmetry, this is equivalent to a collision with a ramp with a slope of $30°$ with respect to the horizontal line.

For sake of simplicity, we consider the equivalent problem in a rectangle, consisting in a rotated shock, whose vertical angle is $30°$. The domain is the rectangle $\Omega = [0,4] \times [0,1]$, whose initial conditions are

$$(\rho, v^x, v^y, E)(x, y, 0) = \begin{cases} \boldsymbol{c}_1 = (\rho_1, v_1^x, v_1^y, E_1) & \text{if } y \leq 1/4 + \tan(\pi/6)x, \\ \boldsymbol{c}_2 = (\rho_2, v_2^x, v_2^y, E_2) & \text{if } y > 1/4 + \tan(\pi/6)x, \end{cases}$$
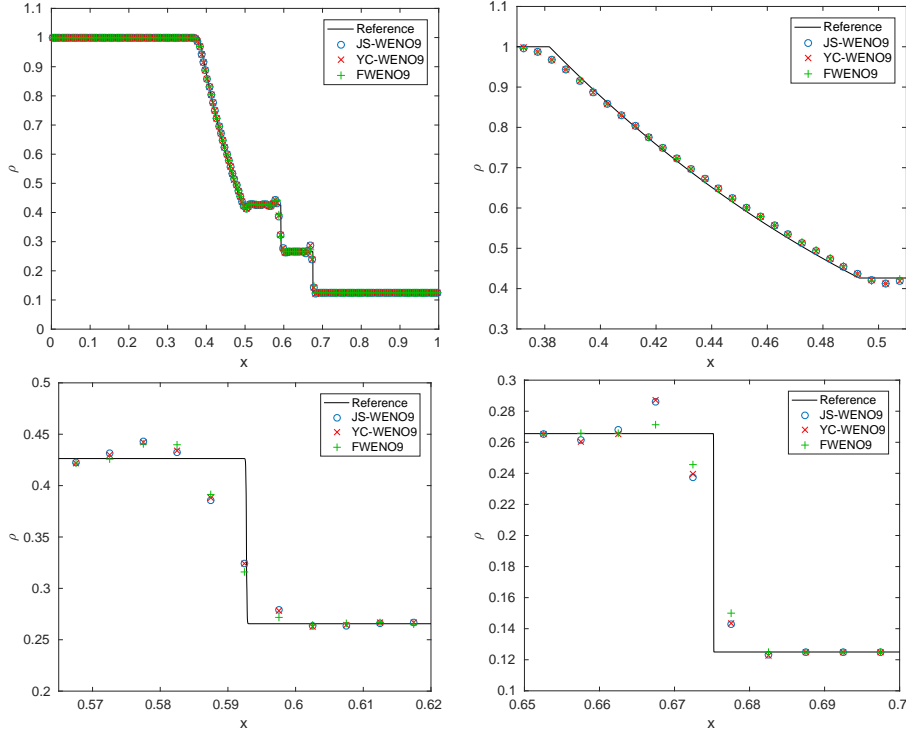
Fig. 8: Example 4 (Sod shock tube problem, 1D Euler equations of gas dynamics): numerical solution for $N = 200$ (top left) and enlarged views (top right, bottom left and bottom right) at $T = 0.1$ produced by ninth-order schemes with conventional (JS-WENO9 and YC-WENO9) and new (FWENO9) smoothness indicators. The reference solution with $N = 100000$ cells is also shown.

$$\boldsymbol{c}_1 = \big(8, 8.25\cos(\pi/6), -8.25\sin(\pi/6), 563.5\big), \quad \boldsymbol{c}_2 = (1.4, 0, 0, 2.5).$$

We impose inflow boundary conditions, with value $\boldsymbol{c}_1$, at the left side, $\{0\} \times [0, 1]$, outflow boundary conditions both at $[0, 1/4] \times \{0\}$ and $\{4\} \times [0, 1]$, reflecting boundary conditions at $(1/4, 4] \times \{0\}$ and inflow boundary conditions at the upper side, $[0, 4] \times \{1\}$, which mimics the shock at its actual traveling speed:

$$(\rho, v^x, v^y, E)(x, 1, t) = \begin{cases} \boldsymbol{c}_1 & \text{if } x \leq 1/4 + (1 + 20t)/\sqrt{3}, \\ \boldsymbol{c}_2 & \text{if } x > 1/4 + (1 + 20t)/\sqrt{3}. \end{cases}$$

We run different simulations until $T = 0.2$ both at a resolution of 2048×512 points and a resolution of 2560×640 points, shown in Figure 10, in both cases with CFL $= 0.4$ and involving the JS-WENO scheme, the YC-WENO method and our FWENO scheme for the case of fifth-order accuracy. The results show that both YC-WENO and FWENO schemes produce sharper resolution than JS-WENO, and in turn they have similar resolution between then.
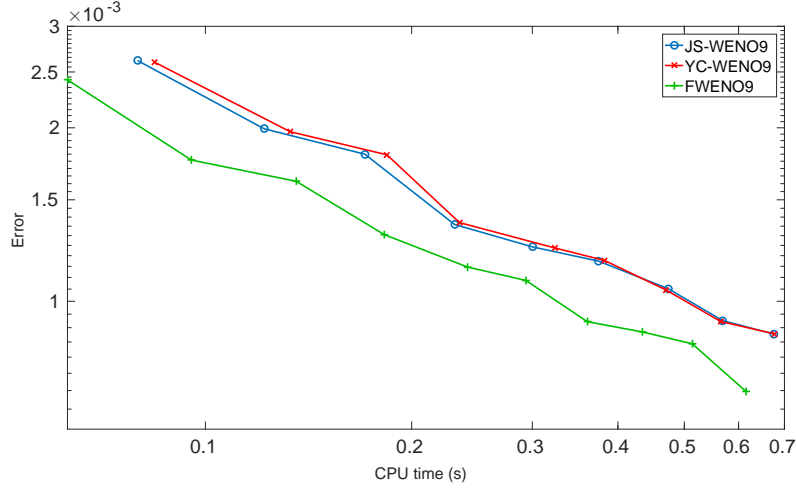
Fig. 9: Example 4 (Sod shock tube problem, 1D Euler equations of gas dynamics): efficiency plot for ninth-order schemes, corresponding to the numerical solution at $T = 0.1$.

Example 6: Riemann problem

Finally, we solve numerically a Riemann problem for the 2D Euler equations on the domain $(0, 1) \times (0, 1)$. Riemann problems for 2D Euler equations were first studied in [7]. The initial data is taken from [5, Sect. 3, Config. 3]:

$$\boldsymbol{u}(x, y, 0) = (\rho(x, y, 0), \rho(x, y, 0)v^x(x, y, 0), \rho(x, y, 0)v^y(x, y, 0), E(x, y, 0))$$

and

$$\begin{pmatrix} \rho(x, y, 0) \\ v^x(x, y, 0) \\ v^y(x, y, 0) \\ p(x, y, 0) \end{pmatrix}^{\mathrm{T}} = \begin{cases} (1.5, 0, 0, 1.5) & \text{for } x > 0.5,\ y > 0.5, \\ (0.5323, 1.206, 0, 0.3) & \text{for } x \leq 0.5,\ y > 0.5, \\ (0.138, 1.206, 1.206, 0.029) & \text{for } x \leq 0.5,\ y \leq 0.5, \\ (0.5323, 0, 1.206, 0.3) & \text{for } x > 0.5,\ y \leq 0.5, \end{cases}$$

with the same equation of state as in the previous test. The simulation is performed taking $s_2 = 2$, with the final time $T = 0.3$, CFL $= 0.4$, resolutions 2048×2048 and 2560×2560 and comparing the same schemes with the same parameters as in Example 5. The results are shown in Figure 11. The same conclusions as in Example 5 are drawn.

We now use the solutions computed with the grid of 2560×2560 points as reference solutions to perform efficiency tests by comparing error versus CPU time involving numerical solutions with grid sizes $16 \cdot 2^n \times 16 \cdot 2^n$, $0 \leq n \leq 4$, for the corresponding fifth, seventh and ninth order schemes. The results are shown in Figure 12 and again indicate a higher performance for the FWENO scheme.

(a) JS-WENO5, 2048×512

(b) YC-WENO5, 2048×512

(c) FWENO5, 2048×512

(d) JS-WENO5, 2560×640

(e) YC-WENO5, 2560×640
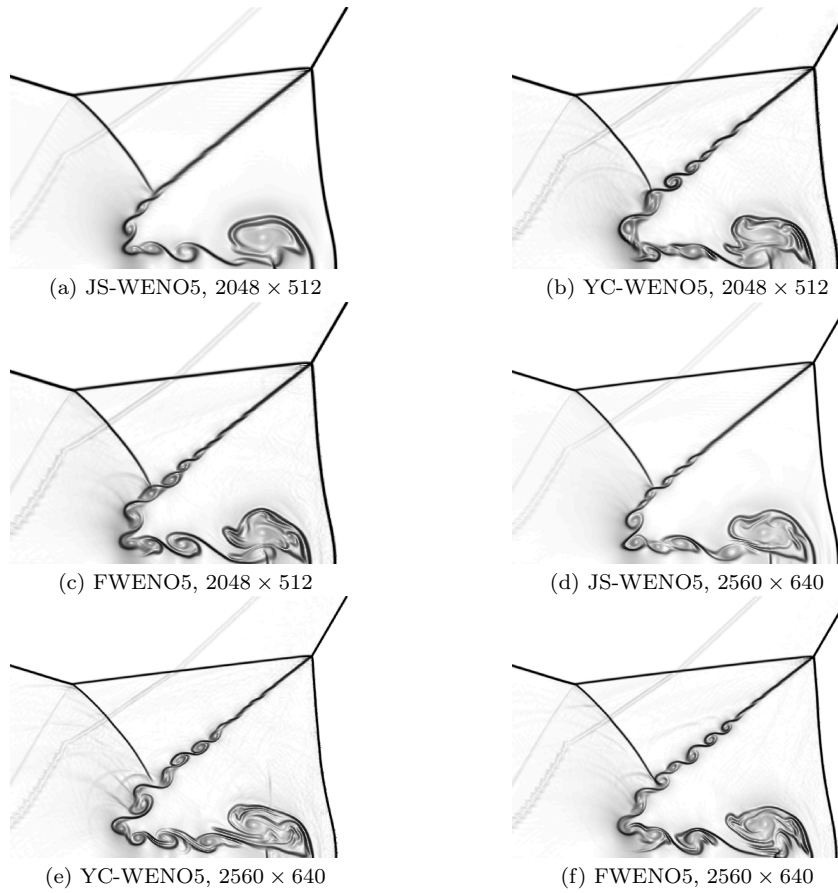
(f) FWENO5, 2560×640

Fig. 10: Example 5 (double Mach reflection, 2D Euler equations of gas dynamics): enlarged views of turbulent zone of numerical solutions at $T = 0.2$ (Schlieren plot).

5 Conclusions

In this paper a set of alternative smoothness indicators, cheaper than the classical Jiang-Shu ones, has been presented. The theoretical results show that when used in Yamaleev-Carpenter type weight constructions they attain the same accuracy properties than the ones obtained with the original smoothness indicators. The numerical experiments confirm all these theoretical considerations. Also, the numerical evidence obtained in the problems from hyperbolic conservation laws with weak solutions also shows that the quality of the approximation is similar in both cases, being the schemes with the modified smoothness indicators (FWENO) more efficient than their traditional counterparts (JS-WENO and YC-WENO).

As for future work, we encompass extrapolating the benefits of this new weight design with the simplified smoothness indicators in the context of WENO extrapolation for numerical boundary conditions and even generalized WENO interpolations/extrapolations in the context of non-uniform grids, in which the compu-

(a) JS-WENO5, 2048 × 2048

(b) YC-WENO5, 2048 × 2048

(c) FWENO5, 2048 × 2048

(d) JS-WENO5, 2560 × 2560

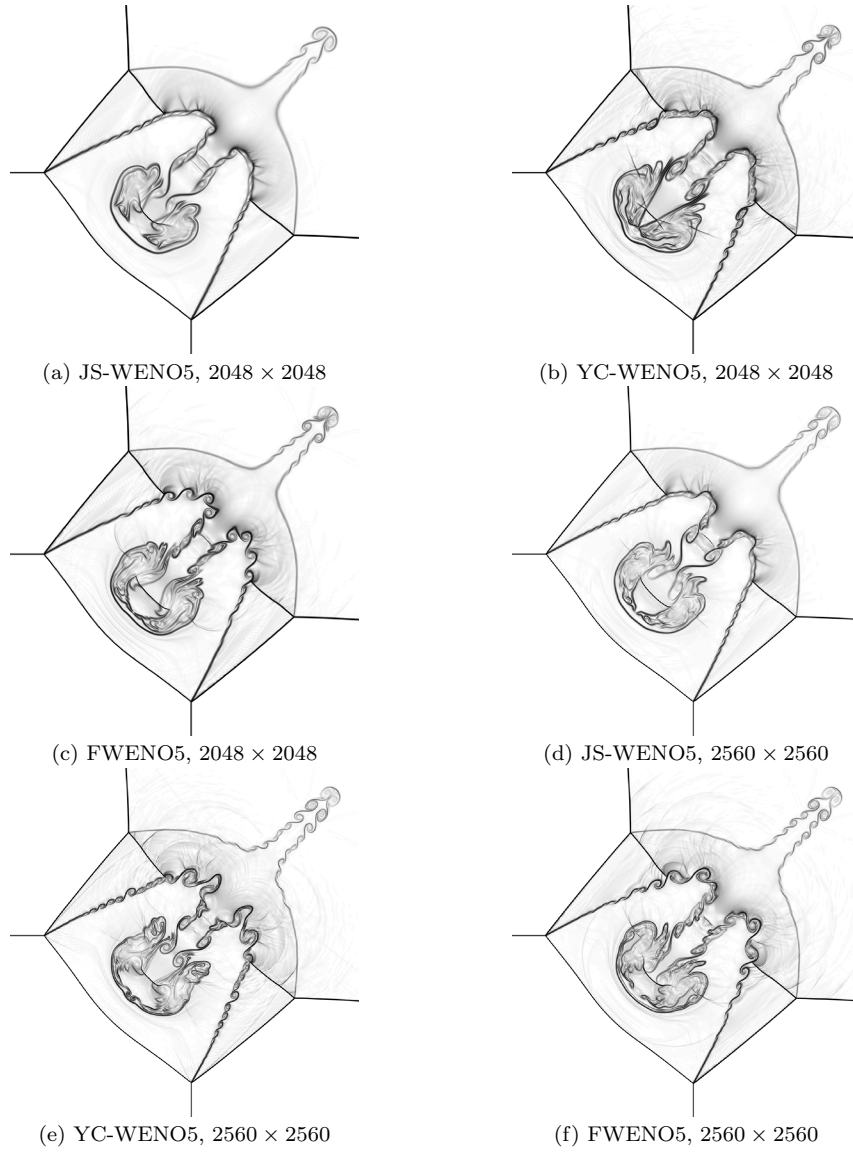(e) YC-WENO5, 2560 × 2560

(f) FWENO5, 2560 × 2560

Fig. 11: Example 6 (Riemann problem, 2D Euler equations of gas dynamics): enlarged views of turbulent zone of numerical solutions at $T = 0.3$ (Schlieren plot).

tational benefits of using these new smoothness indicators with respect to the traditional ones are expected to be much higher than in uniform grids.
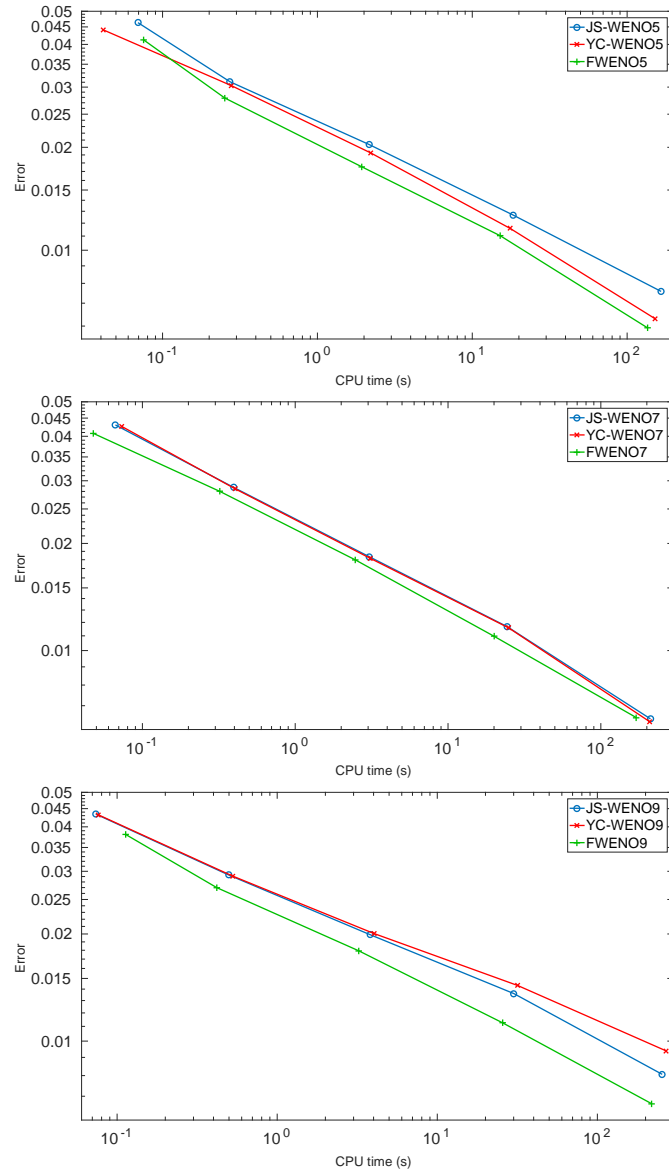
Fig. 12: Example 6 (2D Riemann problem, 2D Euler equations of gas dynamics): efficiency plot for fifth, seventh and ninth-order schemes, corresponding to the numerical solution at $T = 0.3$.

Acknowledgements

References

1. Aràndiga, F., Baeza, A., Belda, A.M., Mulet, P.: Analysis of WENO schemes for full and global accuracy. SIAM J. Numer. Anal. **49**(2), 893–915 (2011)
2. Bürger, R., Kenettinkara, S. K., Zorío, D.: Approximate Lax-Wendroff discontinuous Galerkin methods for hyperbolic conservation laws. Computers & Mathematics with Applications, **74**(6), 1288–1310 (2017)
3. Donat, R., Marquina, A.: Capturing shock reflections: An improved flux formula. J. Comput. Phys. **125**, 42–58 (1996)
4. Jiang, G.S., Shu, C.W.: Efficient implementation of Weighted ENO schemes. J. Of Comput. Phys. **126**, 202–228 (1996)
5. Kurganov, A., Tadmor, E.: Solution of two-dimensional Riemann problems for gas dynamics without Riemann problem solvers Numer. Methods Partial Differential Equations **18**, 584–608 (2002)
6. Liu, X-D., Osher, S., Chan, T.: Weighted essentially non-oscillatory schemes. J. Comput. Phys. **115**(1) 200–212 (1994)
7. Schulz-Rinne, C. W.: Classification of the Riemann problem for two-dimensional gas dynamics. SIAM Journal on Mathematical Analysis **24**(1), 76–88 (1993)
8. Shu, C.-W., Osher, S.: Efficient implementation of essentially non-oscillatory shock-capturing schemes. J. Comput. Phys. **77**, 439–471 (1988)
9. Shu, C.-W., Osher, S.: Efficient implementation of essentially non-oscillatory shock-capturing schemes, II. J. Comput. Phys. **83**(1), 32–78 (1989)
10. Shu, C.-W.: Essentially non-oscillatory and weighted essentially non-oscillatory schemes for hyperbolic conservation laws. In Cockburn, B., Johnson, C., Shu, C.-W. and Tadmor, E. (Quarteroni, A., Ed.): Advanced Numerical Approximation of Nonlinear Hyperbolic Equations. Lecture Notes in Mathematics, vol. 1697, Springer-Verlag, Berlin, 325–432 (1998)
11. Sod, G. A.: A survey of several finite difference methods for systems of nonlinear hyperbolic conservation laws. J. Comput. Phys. **27**(1), 1–31 (1978)
12. Yamaleev, N. K., Carpenter, M. H.: Third-order Energy Stable WENO scheme. J. Comput. Phys. **228**(8), 3025–3047 (2009)
13. Yamaleev, N. K., Carpenter, M. H.: A systematic methodology to for constructing high-order energy stable WENO schemes. J. Comput. Phys. **228**(11), 4248–4272 (2009)